Compact Planar Beamforming Array with End-Fire Radiating Elements for 5G Applications

Maral Ansari, *Student Member, IEEE*, He Zhu, *Member, IEEE*, Negin Shariati, *Member, IEEE*, and Y. Jay Guo, *Fellow, IEEE*

***Abstract*—In this paper, a compact 4 × 6 Butler matrix (BM) based on microstrip lines is designed and applied to a linear antenna array. The proposed design creates four beams in four different directions within the 27.5 GHz and 28.5 GHz band. One of the advantages of this BM is a reduction in the size of the beamforming network (BFN). In order to attain this objective, the basic microstrip-based 4 × 4 BM is designed, and then modified to a 4 × 6 BM through a dual-substrate structure to avoid crossing lines using microstrip-to-slotline transitions. The BFN is cascaded with a 6-element linear antenna array with end-fire radiating elements. The array can be conveniently integrated into the BFN. The resulting design benefits from low loss characteristics, ease of realization, and low fabrication cost. The array is fabricated and tested, and the experimental results are in good agreement with the simulated ones. The multi-beam antenna size is $5.6\lambda \times 4.6\lambda$ including feed lines and feed network, while the new BM design is only $3.5\lambda_0 \times 1.4\lambda_0$, which is almost half as large as the traditional one. The measured radiation patterns show that the beams cover roughly a spatial range of 90° with a peak active gain of 11 dBi.**

***Index Terms*—Antenna array, beamforming network (BFN), Butler matrix (BM), end-fire, fifth-generation (5G)**

I. Introduction

THE global demand for high capacity and higher data rate wireless communication is growing at a startling pace. This traffic surge will entail the exploration of the underutilized millimeter wave (mm-wave) frequency spectrum for potential application in future [1], [2]. Consequently, frequencies around 28 GHz are expected to be used increasingly in future cellular systems of the fifth-generation (5G) [3].

A beamforming antenna array can create multi-beams in an angular area, increasing capacity as it can serve different users by different beams [4]–[9]. In the design of a beamforming network (BFN) desirable features are simplicity, low cost design, low losses, and most notably compactness and easy integration to the antenna to reduce the number of components. Compared to the beamforming techniques such as: Nolen matrix [10], Blass Matrix [11] and Rotman lens [12], the Butler matrix (BM) has been the more popular since it requires the least number of components, and is theoretically lossless [13].

Typically, 4 × 4 Butler matrices are the most common form, because of their relatively simple network [14]–[17]. Design of Butler matrices with more outputs are quite promising due to the ability to provide lower sidelobe levels (SLL), lower crossover level, high directional and narrower beams [18]–[23]. In general, Butler matrices are designed using hybrid couplers, fixed phase shifters and crossovers. Such structures are bulky and may have poor performance, mainly because of the crossovers employed. Specific designs have been suggested to avoid using crossovers. In [16] a 4 × 4 BM with the slot-coupled directional coupler, using coplanar waveguide (CPW) multilayer technology operating at 5.8 GHz is described. Another low cost mm-wave 4 × 4 microstrip BM is presented in [17], without any crossovers on single-layer substrate, but it is not scalable to 8 × 8 matrices and layers.

Different conceivable solutions have been proposed to avoid crossovers in the structure such as: air-bridge technique [17], and plate-through via-hole. These schemes all have shortcomings. The former technique entails an asymmetrical structure, and as a result introduces unwanted coupling, while the latter requires great accuracy and is costly to realize, especially on thin dielectrics. Besides, operating at mm-wave frequencies, these techniques may require extra elements to compensate the parasitic effects of via or bridge. Moreover, the use of wire-bonding or non-planar structures complicates the fabrication process and are technologically difficult to realize, expensive and may reduce yield.

In this paper, a 6-element linear antenna array fed by a compact 4 × 6 BM based on microstrip lines is used for beam steering at 28 GHz for future 5G cellular networks. A simplified BM is proposed to reduce the size of the traditional BM by using a fewer number of crossovers. Starting with 4 × 4 BM, we extended the number of elements from 4 to 6. This lengthens the array, increases the gain and reduces side lobe level [14]–[17]. Compared to 4 × 8 and 8 × 8 Butler matrices [19]–[24], the structure is obviously simpler and uses fewer crossovers. Our method can be applied to design 4 × 8 and 8 × 8 Butler matrices as well. Furthermore, the use of microstrip technology for its realization is attractive due to its light weight, low profile, low cost, and ease of integration.

The presented BM design consists of new crossover configuration, which avoids the complexity of other structures. Fig. 1 compares the traditional 4 × 6 BM design [18] with the proposed structure of the 4 × 6 BM with fewer components. The single element is a microstrip-fed dual-layer half-wavelength dipole with a director chosen for its simple structure, high directional and end-fire radiation pattern. The array is properly tapered in order to reduce the side-lobes, and the BFN phases the antenna elements for beam switching capabilities.

Manuscript submitted January 30, 2019; revised May 27, 2019, Accepted June 13, 2019.

The authors are with the Global Big Data Technologies Centre (GBDTC), University of Technology Sydney, Ultimo, NSW 2007, Australia (email: Maral.ansari@student.uts.edu.au)

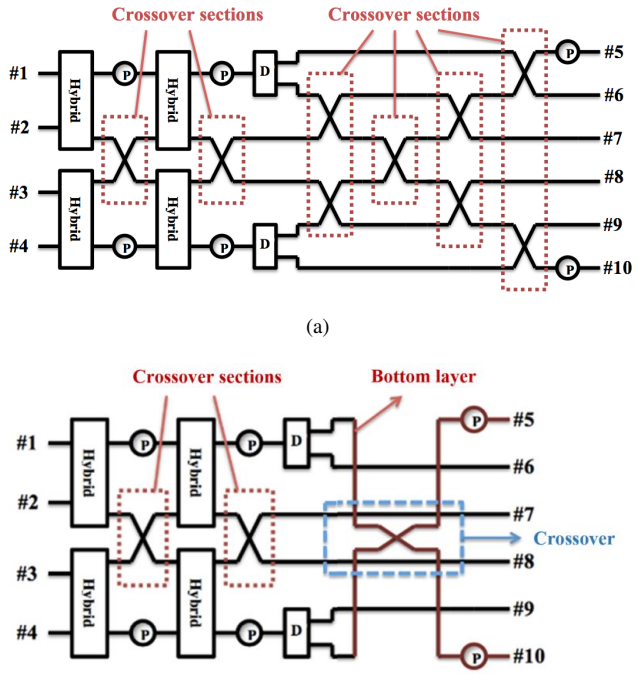

Fig. 1. Block diagram of the 4 × 6 BM. (a) Traditional 4 × 6 BM. (b) Proposed 4 × 6 BM.

The remainder of the paper is organized as follows. In section II, a simple and compact 4 × 6 BM based on microstrip lines at 28 GHz is presented. The design and performance of the antenna array integrated with its BFN is described in section III. In the following section, the correspondence between experimental and simulated results is evaluated. Finally, in the last section, conclusions are drawn.

II. Simplified 4 × 6 Butler Matrix Using Microstrip-to-Slotline Transition

In this section, the design and analysis of 4 × 6 BM is described, and the proposed structure which has some novel design features is illustrated. The traditional 4 × 6 BM and the new configuration consisting of fewer components are depicted in detail. The simulated results of the BFN are also shown.

A. 4 × 6 *Butler Matrix Analysis*

The scattering matrix of a 4×6 BM with ports 1, 2, 3, and 4 as inputs and ports 5, 6, 7, 8, 9, and 10 as outputs can be written as:

$$[S] = \begin{bmatrix} [0]_{4\times4} & [S_r]^T_{4\times6} \\ [S_r]_{6\times4} & [0]_{6\times6} \end{bmatrix} \tag{1}$$

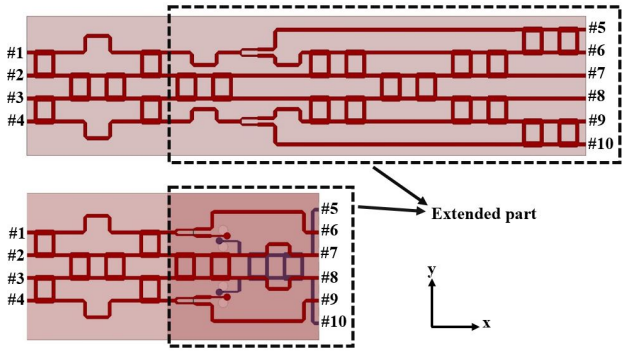

Fig. 2. Comparison of the traditional 4 × 6 BM structure with the proposed design.

where, $[S_r]_{6\times4} =$

$$\frac{1}{2}\begin{bmatrix} \frac{1}{\sqrt{2}}e^{+j\frac{1}{4}\pi} & \frac{1}{\sqrt{2}}e^{+j\frac{1}{2}\pi} & \frac{1}{\sqrt{2}}e^{+j\frac{1}{4}\pi} & \frac{1}{\sqrt{2}}e^{-j\pi} \\ \frac{1}{\sqrt{2}} & \frac{1}{\sqrt{2}}e^{-j\frac{3}{4}\pi} & \frac{1}{\sqrt{2}}e^{-j\frac{1}{2}\pi} & \frac{1}{\sqrt{2}}e^{-j\frac{3}{4}\pi} \\ e^{-j\frac{1}{4}\pi} & 1 & e^{-j\frac{5}{4}\pi} & e^{-j\frac{1}{2}\pi} \\ e^{-j\frac{1}{2}\pi} & e^{-j\frac{5}{4}\pi} & 1 & e^{-j\frac{1}{4}\pi} \\ \frac{1}{\sqrt{2}}e^{-j\frac{3}{4}\pi} & \frac{1}{\sqrt{2}}e^{-j\frac{1}{2}\pi} & \frac{1}{\sqrt{2}}e^{-j\frac{3}{4}\pi} & \frac{1}{\sqrt{2}} \\ \frac{1}{\sqrt{2}}e^{-j\pi} & \frac{1}{\sqrt{2}}e^{+j\frac{1}{4}\pi} & \frac{1}{\sqrt{2}}e^{+j\frac{1}{2}\pi} & \frac{1}{\sqrt{2}}e^{+j\frac{1}{4}\pi} \end{bmatrix} \tag{2}$$

Equation (2) clarifies the design considerations of a 4 × 6 BM as well as indicating the magnitude and phase of each outputs. From (2) one can see that the phase differences between any two adjacent elements of each column are $-\pi/4$, $+3\pi/4$, $-3\pi/4$, and $+\pi/4$, respectively. The coefficient of $1/2$ appears because of two equal-power hybrids. From designing point of view, there should be two 3 dB power dividers to implement $1/\sqrt{2}$ power appearing in the first two and last two rows of matrix together with two phase shifters to be applied to the output ports 5 and 10 to realize 180° phase shifts.

B. *Design Consideration of the* 4 × 6 *Butler Matrix*

In order to construct such a beamforming network, hybrid couplers and fixed phase shifters are required to provide appropriate power division and phase at each output port. According to the above analysis, the proposed 4 × 6 BM can be configured as Fig. 1(b), while the newly structure is divided into two layers, the top layer, and the bottom one, which is displayed by red lines. Fig. 2 compares the complexity and size of the traditional 4 × 6 BM and the new one. First, the basic 4 × 4 BM is designed, then, it is extended to a 4 × 6 BM. The extended part is indicated by the dashed box.

In Fig. 3 the schematic of the new design is shown in details, and the geometries of the final design of BFN are

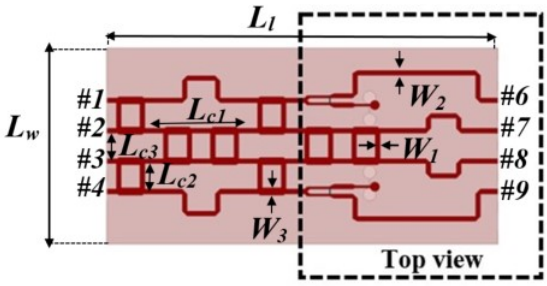

(a)

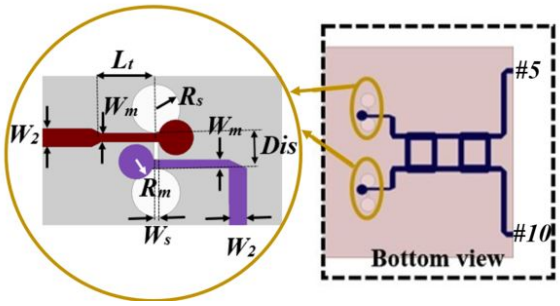

(b)

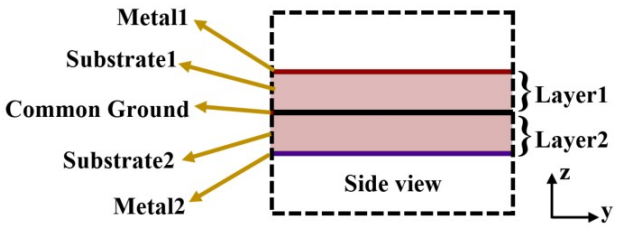

(c)

Fig. 3. Geometries of the proposed 4 × 6 BM with the schematic of cross section. (a) Top view. (b) Bottom view and zoomed out of the microstrip transition part. (c) Side view and schematic of cross section.

TABLE I
DIMENSIONS OF THE 4 × 6 BUTLER MATRIX (UNIT:MM)

L_{c1}	7.2	R_s	0.55	W_1	0.2
L_{c2}	2.06	R_m	0.4	W_2	0.41
L_{c3}	2.62	W_s	0.1	W_3	0.64
L_w	13.5	W_m	0.19	Dis	0.7
L_l	30.5	L_t	2.2	h	0.127

also shown. Besides, the design parameters are listed in Table I. As mentioned before, the BFN is a two layer structure. Four input ports 1-4 and four output ports 6-9, are located on layer 1, while two of the output ports 5 and 10 are on layer 2. Layer 1 of BM consists of four hybrid couplers, two 45° phase shifters, two crossovers, and two 3 dB Wilkinson power dividers. Layer 2 is constructed using only one crossover. The signal is coupled from layer 1 to layer 2 through two microstrip-to-slotline transitions. The slot is located on their common ground plane, and its parameters are specified to minimize the network loss.

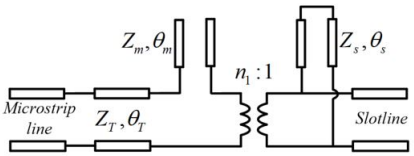

(a)

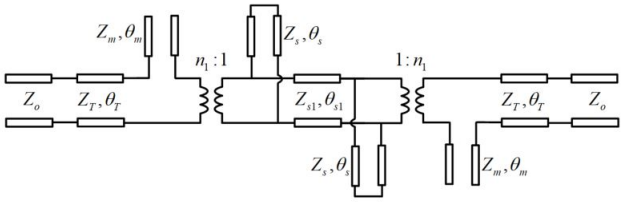

(b)

Fig. 4. Equivalent circuits of (a) the microstrip-to-slotline transition; (b) the microstrip-slotline-microstrip transition.

In contrast to the size of conventional 4 × 6 BM, the new design is smaller by almost 50%, while having a good overall performance. In this structure, some of the selected transmission-line crossovers in Fig. 1 are realized by microstrip-to-slotline transitions. Such technology untangles the problem of bulky crossover couplers [25], and is compatible with ordinary microstrip circuits. The end result is that seven of the crossovers are replaced by one crossover and two transitions. This achieves a compact structure with the minimum number of coupled-line sections plus a common ground and using no interlayer nor any connections.

In order to achieve minimum loss, a substrate with very low loss tangent and small dielectric constant is employed. However, in this case, the radius of curvature in the bend and the line width are increased, so a very thin dielectric is desired [19]. Components are designed on Rogers 5880, with a 127-micrometer thickness of dielectric for both layers. This provides the best performance for the BM, and maintains feasible feature size for fabrication.

C. Microstrip-to-slotline Transition

The microstrip-to-slotline transition is the most common way in which an RF signal is coupled between two sides of planar dielectric structure [25], [26]. The microstrip-to-slotline transition can also avoid unwanted bonding wires or metal vias that may increase the cost and complexity of manufacture. In this design, microstrip-to-slotline transitions are using different metal layers to work as crossovers, which render two major advantages to the structure: one is to reduce the number of crossovers compared with the traditional topology, and the other one is to maintain good isolation between two signals. The microstrip-to-slotline transition part of the circuit is zoomed out in Fig. 3(b), where the microstrip lines in red and purple are actually located on different metal layers, and the slotline is on the common ground. Fig. 3(c) shows the side-view of the substrate, which illustrates the layer

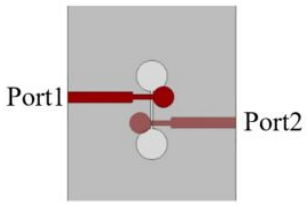

Fig. 5. Configuration of the designed crossover using a microstrip-slotline-microstrip transition.

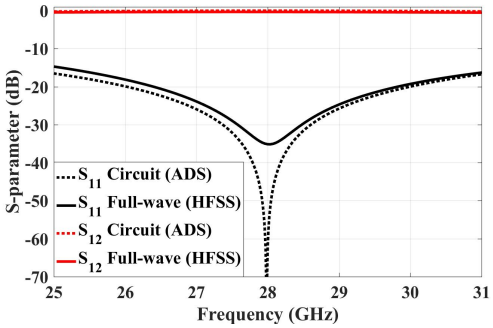

Fig. 6. Simulated performance of the microstrip-slotline-microstrip transition.

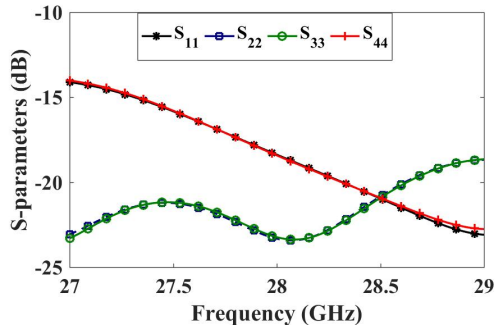

(a)

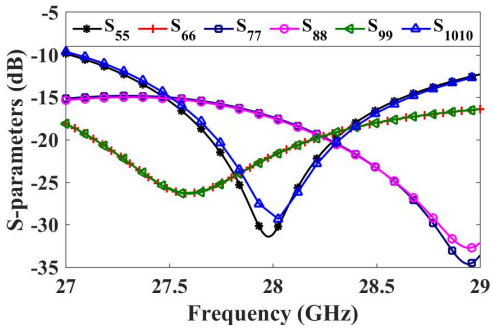

(b)

Fig. 7. Simulated S-parameters of the 4 × 6 BM. (a) Magnitude of reflection coefficients of inputs versus frequency. (b) Magnitude of reflection coefficients of outputs versus frequency.

distribution of the metals and substrates. It is noted that 180° phase shift of the two outputs (port 5 and port 10) compared with other two outputs (port 9 and port 6) is introduced, due to the inverted electrical field distribution caused by the microstrip-to-slotline transition.

Fig. 4(a) and (b) show the simplified equivalent circuit of the microstrip-to-slotline transition and the crossover, respectively. The microstrip-to-slotline transition consists of a transmission line (Z_T,θ_T), a series radical microstrip stub (Z_m,θ_m) ended with open circuit, a power transformer with turns ratio of $n_1 : 1$, and a shunted short-stub (Z_s,θ_s). The electrical lengths of θ_m and θ_s are all set to a quarter-wavelength at f_0. In this case, the stub becomes a quarter-wavelength open-ended stubs, which can be considered as a virtual short circuit. Similarly, the quarter-wavelength short-ended slot stub can be considered as a virtual open circuit. Therefore, to determine the dimensions and performance of the circuit, a simplified model including the characteristic impedances of the slotline Z_{slot} and the microstrip line Z_{ms} , and transformer's ratio (n_1) can be used, and the relation between them is $Z_{ms} = n_1^2 \cdot Z_{slot}$. The width of the slotline should not be too narrow to avoid problems with the manufacturing errors [27], and its length should be adjusted to obtain a low insertion loss. To this end, the slotline impedance is chosen as 100 Ω with the length of $Dis = \lambda/14$ (at 28 GHz). The transmission line (Z_T,θ_T) works as an impedance transformer to match the impedance from the microstrip-to-slotline transition to the microstrip line Z_0. Therefore, to achieve a good matching from the microstrip line, impedance of the quarter-wavelength transformer can be determined by $Z_T = \sqrt{Z_o \cdot Z_{ms}} = 70.7$ Ω. In summary, the relevant parameters in the equivalent circuit are chosen as: $\theta_T = 15°$, $\theta_s = 90°$, $\theta_{s1} = 90°$, $\theta_m = 90°$, $Z_T = 70.7$ Ω, $Z_s = 126.5$ Ω, $Z_{s1} = 100$ Ω, and $Z_m = 75.8$ Ω.

Fig. 5 shows the configuration of the designed crossover using a microstrip-slotline-microstrip configuration. The two microstrip lines are located on different metal layers and the slotline is on the middle ground. The dimensions of the structure are chosen according to the equivalent circuit. To demonstrate the performance and advantage of this transition-based crossover and its operation, the comparison between the circuit simulation in ADS and full-wave one in HFSS is conducted, as shown in Fig. 6. It is observed that two results agree very well. The microstrip-slotline-microstrip transition shows 0.3 dB insertion loss, and a return loss better than 25 dB within the bandwidth. It is noticeable that in this design, only limited bandwidth is considered when selecting the related parameters, but the microstrip-to-slotline transition can realize an extended bandwidth if it is required during the design process.

D. Butler Matrix Components

Apart from the microstrip-to-slotline transition, to build a BM, there are some other components required including couplers, phase shifters and power dividers. The 3 dB hybrid couplers are designed at 28 GHz for 50 Ω microstrip lines, in which structure the input power is equally divided between the output ports with a 90° phase difference, and maximum isolation between its coupling ports. The isolation between coupling ports and the magnitude of reflection coefficient for input ports are less than -30 dB over the desired bandwidth.

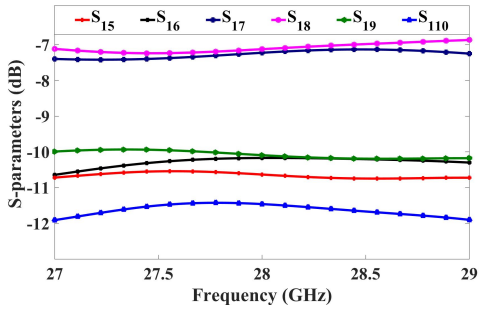

(a)

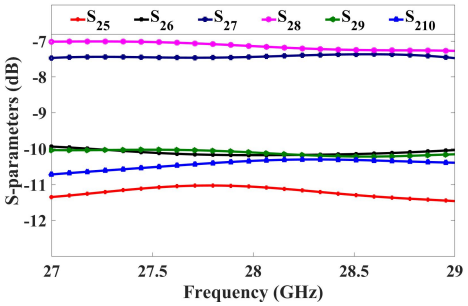

(b)

Fig. 8. Simulated S-parameters of the 4 × 6 BM versus frequency. (a) Magnitude of the outputs power when port 1 is fed. (b) Magnitude of the outputs power when port 2 is fed.

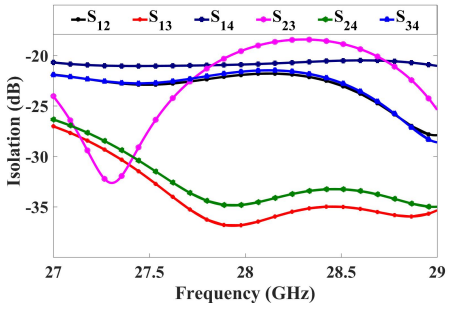

(a)

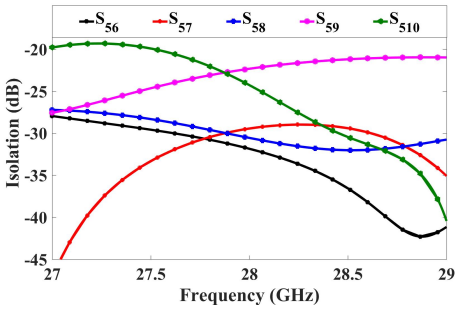

(b)

Fig. 9. Simulated S-parameters of the 4 × 6 BM. (a) Isolation of inputs versus frequency. (b) Isolation of outputs versus frequency.

The delay line phase shifters fulfill the required phase shift at the output signals. Two 3 dB Wilkinson power dividers split the signal power at the first and last outputs (ports 5 and 10) to make six outputs out of four outputs coming from the first stage, which is the basic 4 × 4 BM.

Finally, the crossovers between the lines must be considered. The microstrip branch-line crossovers satisfy the requirements for the basic 4 × 4 BM part. On the other hand, in the extended 4 × 6 BM, using too many crossovers would result in bulky and lossy structure. As mentioned in the section II-C, the microstrip-to-slotline transition is the technology that is chosen instead of alternative branch-line crossover. In the proposed configuration, four couplers are combined and some of the crossovers are effectively avoided. Also, two of phase shifters are omitted from the structure, since the required phase shift can be obtained through the power dividers and transitions. In this case, the overall circuit size and loss are effectively reduced.

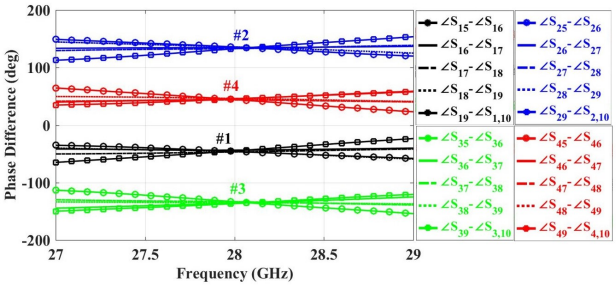

Fig. 10. Simulated phase difference at the output ports of the BFN versus frequency with respect to that of port 1, 2, 3, 4 being fed.

The BFN is simulated with the full electromagnetic package HFSS. Fig. 7 shows the simulated magnitude of the reflection coefficients of the input and output ports of the BFN. Fig. 8 and Fig. 9 indicate the insertion loss and isolation between ports, respectively. As the structure is symmetric, the results for ports 3 and 4 are similar to those of ports 1 and 2. Fig. 10 represents a frequency-dependent phase. The progressive phase shift of $-45° \pm 7°$, $+135° \pm 10°$, $+45° \pm 7°$, $-135° \pm 10°$ are obtained by feeding port 1 to port 4, respectively. The design is optimized to have a minimum phase error at 28 GHz. The newly designed BFN exhibits an average insertion loss of 2.4 dB with amplitude variation less than 0.53 dB and an average phase imbalance of less than $10°$ from 27.5 to 28.5 GHz, 1 GHz bandwidth, which completely covers the 27.5 to 28.35 GHz band proposed for future 5G cellular systems. The circuit size is only $1.4\lambda_0 \times 3.5\lambda_0$ excluding the length of feed lines. This corresponds to a very significant miniaturization in the size and notable simplification in the design compare to the traditional BM. The reflection coefficients are better than -15 dB within the design bandwidth and good isolation is observed between ports (< -20 dB) within this band.

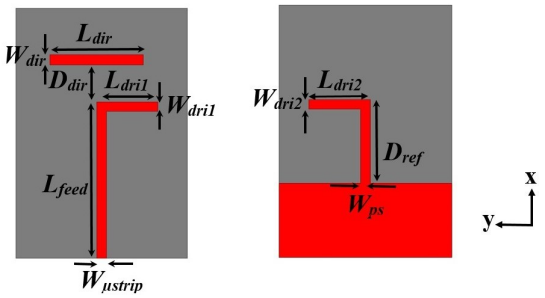

(a) (b)

Fig. 11. Geometry of the proposed single element antenna design. (a) Top view. (b) Middle layer view (Butler matrix ground layer).

TABLE II
DIMENSIONS OF THE ANTENNA (UNIT:MM)

L_{feed}	5	L_{dri1}	2.1	$W_{\mu trip}$	0.41
L_{dir}	3.2	W_{dri1}	0.39	W_{ps}	0.41
W_{dir}	0.41	L_{dir2}	2.2	D_{ref}	2.7
D_{dir}	1.9	W_{dir2}	0.39		

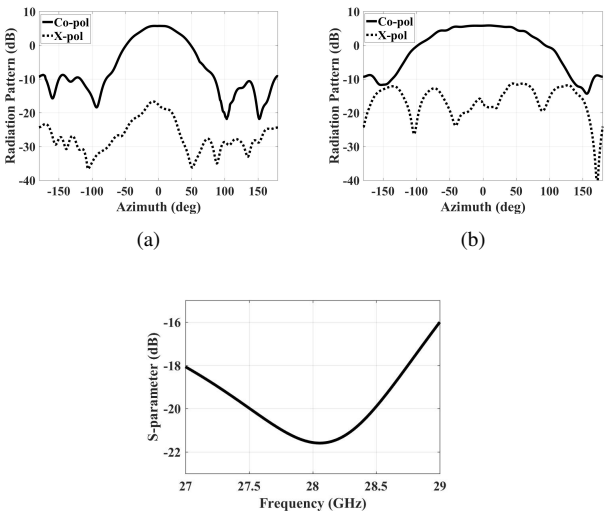

(a) (b)

(c)

Fig. 12. Simulated results of the proposed single element antenna. (a) Co-polarization (co-pol) and cross-polarization (x-pol) at E-plane. (b) Co-polarization and cross-polarization at H-plane. (c) Reflection coefficient.

III. DIPOLE ARRAY INTEGRATED WITH BUTLER MATRIX

In this section, a 6-element linear planar microstrip-fed dipole array is designed at 28 GHz. The proposed modified 4×6 BM is cascaded with this array to study the beam switching capability through the investigation of how the distributions of the phase and magnitude affect the radiation pattern within the entire frequency band. The amplitude tapering along with each element phasing is provided by the 4×6 BM to the antenna array, so imposes SLL control along with narrower beams and better crossover level between adjacent beams. It should be noted that multi-beam antennas with crossover level less than -3 dB are needed for 5G base station antennas.

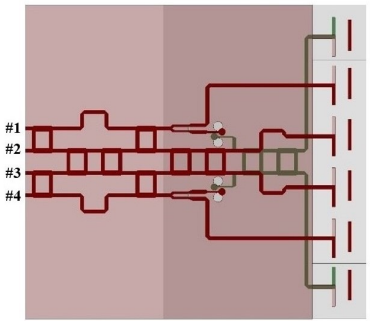

Fig. 13. Geometry of the overall circuit including beamforming network cascaded with the antenna array.

A. Element Design and Performance

A microstrip-fed planar dipole element has been successfully modeled and analyzed. It is chosen due to its simplicity, ease of fabrication, attractive radiation characteristics like end-fire pattern and low cross polarization level [28]. The design is operating at Ka band. Hence, it is very small in size. Although the simple dipole antenna suffers from narrow bandwidth, in this work, the proposed one completely covers the design bandwidth of 27.5 to 28.5 GHz.

In Fig. 11 the single element antenna design is illustrated, while Table II categorizes the dimensions of the proposed antenna. Such antennas often require a sophisticated balun for transformation of RF signals into the microstrip circuit [29]. However, in this work, the driver is fed by two parallel striplines. One of them located on the top layer is connected to one half of dipoles, and the other one on the ground is cascaded to the microstrip line of the feed directly. In addition, a planar director is also utilized to improve the antenna gain.

By employing the proposed antenna in the array and cascading into the presented feed network, there is not a necessity for using balun to feed, but also the ground plane added from the feed network helps to achieve high front-to-back (F/B) gain ratio in the radiation pattern. Unbalance is small across the required bandwidth. Therefore, this antenna design is easily integrated into microstrip circuits, while possessing an end-fire radiation pattern.

Design and full-wave analysis of the antenna were performed using HFSS. The diagrams in Fig. 12 provide information about the gain and magnitude of reflection coefficient of the single element antenna. These plots show that the simulated peak gain is 6.3 dBi at 28 GHz, while the 3 dB beamwidth of the radiation pattern is 72°. The maximum cross-polarization level is –22 dB, and the reflection coefficient is better than -20 dB from 27.5 to 28.5 GHz.

B. Antenna Array and the Complete Network

The antenna is used as a single element of the antenna array. The BM is integrated into the array to realize the beamforming antenna array. Fig. 13 shows the simulated structure of the

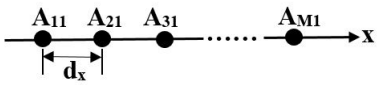

Fig. 14. Linear antenna array

complete network. The array inter-element spacing of 5.8 mm is imposed, which corresponds to $0.58\lambda_0$ at the design center frequency (28 GHz). This was found through a compromise between minimum SLL and grating lobe. It is of significance to mention due to the presence of the BM ground, the ground of the array is not required when the array is cascaded with the BFN. Four of the array elements are integrated into the top layer of BM, and two of them located in the ends are integrated in the bottom layer. However, such thin substrate thickness, 1/36 λ, does not make a noticeable difference between the proposed array and a totally linear array. To verify the working principle of this network, a basic linear array, as shown in Fig. 14 is discussed.

The amplitude of the M^{th} output port of the $N \times M$ BM is represented as A_M , and ϕ_x is the progressive phase difference. Suppose that this array is fed by such an $N \times M$ BM, the array factor of the linear array in (3) can be expressed as:

$$S_x(\theta_x) = \sum_{n=1}^{M} A_m e^{-jnu_x} \tag{3}$$

where, $u_x = kd_x \cos\theta_x + \phi_x$. k is the propagation constant in the free space, d_x stands for the distance between adjacent antenna elements, and θ_x refers to the orientation angle. Based on aforesaid theory, the prediction of the point source six element linear array is calculated to study the effect of mutual coupling on the antenna array [30]. Fig. 15 compares the radiation patterns of the 6-element array. Three scenarios are considered when single ports 1, 2, 3, and 4 of the BM are fed, and for the array case when phase increment between each antenna element is equal to $-45°$,$+135°$,$-135°$, and $+45°$, respectively. First, ideal array with point sources having the same phase and amplitude distribution with the BFN is considered. The matrix A_M in (4) represents the amplitude distribution of the first scenario.

$$A_M = \begin{bmatrix} A_1 \\ A_2 \\ A_3 \\ A_4 \\ A_5 \\ A_6 \end{bmatrix} = \begin{bmatrix} 0.707 \\ 0.707 \\ 1 \\ 1 \\ 0.707 \\ 0.707 \end{bmatrix} \tag{4}$$

From a mathematical point of view, the matrix form of the output signal of a $N \times M$ BM can be shown as vector A_x :

$$A_x = \begin{bmatrix} A_{x1} \\ A_{x2} \\ \vdots \\ A_{xM} \end{bmatrix} = \begin{bmatrix} A_1 e^{-j\phi_x} \\ A_2 e^{-2j\phi_x} \\ \vdots \\ A_M e^{-Mj\phi_x} \end{bmatrix} \tag{5}$$

Array with point sources is used as the ideal one which is simulated in Matlab to compare with two other scenarios.

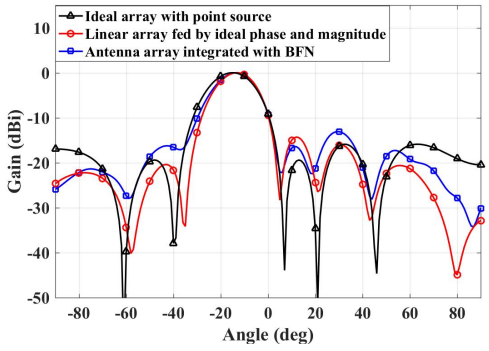

(a)

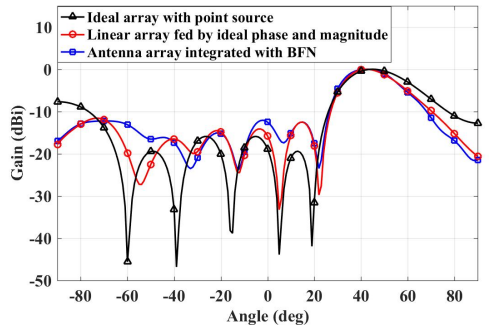

(b)

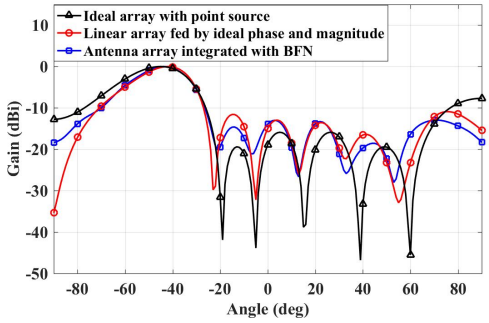

(c)

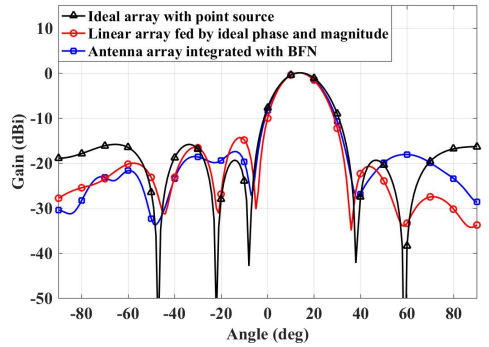

(d)

Fig. 15. Simulated radiation patterns of the multi-beam antenna corresponding to three scenarios including ideal array with point sources, linear array with ideal amplitude and phase, antenna array integrated with BM at 28 GHz. (a) Port 1 is fed. (b) Port 2 is fed. (c) Port 3 is fed. (d) Port 4 is fed.

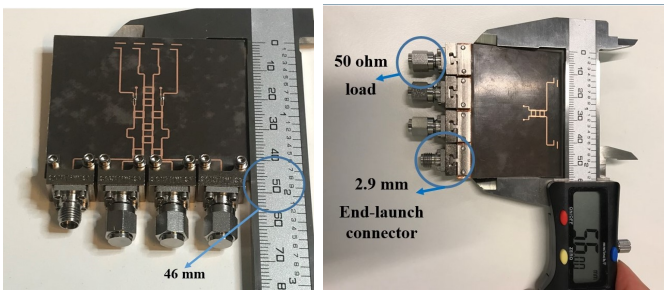

(a) (b)

Fig. 16. Photographs of the fabricated multi-beam array antenna. (a) Top view. (b) Bottom view

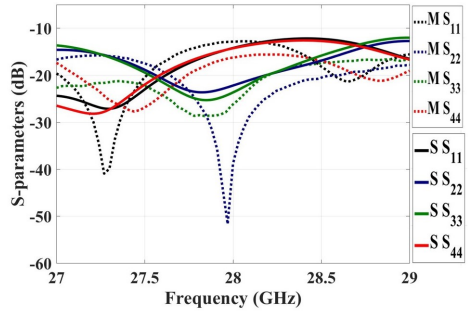

(a)

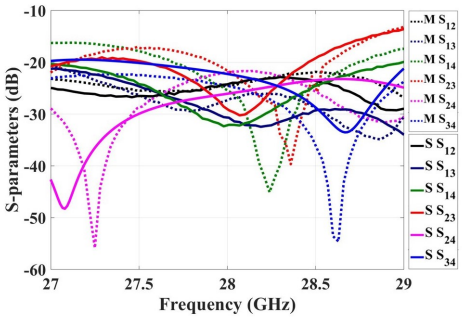

(b)

Fig. 17. Simulated and measurement results for all 4 input ports. (a) Reflection coefficients. (b) Isolation coefficients. The solid lines represent the simulated results and the dashed ones show the measured outcomes.

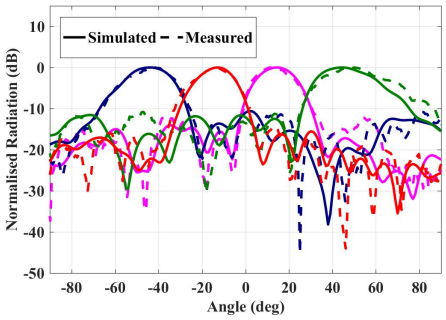

(a)

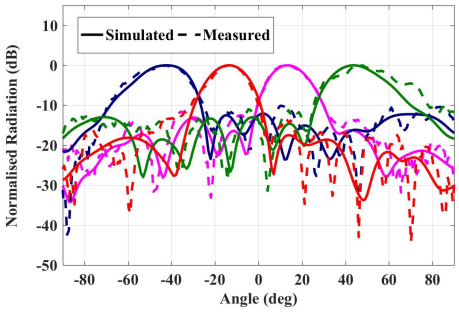

(b)

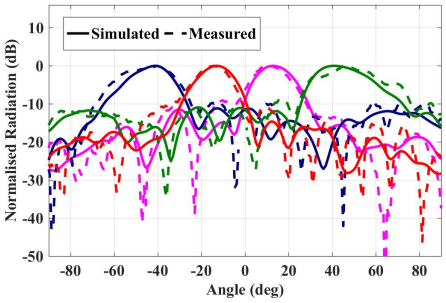

(c)

Fig. 18. Simulated and measured E-plane patterns of the 6-element linear antenna array with incorporated BM corresponding to the four input ports (from left to right when port 2, 1, 4, 3 are fed, respectively) (a) f = 27.5 GHz. (b) f = 28 GHz. (c) f = 28.5 GHz.

In the second scenario, the 6-element linear antenna array is simulated in HFSS, each element is fed with the same amplitude and phase distribution as the BM model, similar to the phase and amplitude distribution of the previous case. By comparing this case with the previous one, the effect of mutual coupling is investigated. Finally, the antenna array fed by the BM is employed to evaluate the BM imperfection through comparison of the last two cases. Evaluations of these graphs indicate that the mutual coupling does not cause severe degradation of the performance of array's patterns, and also show that the BM satisfies design requirements and is working as intended.

This design can be conducted by completing the following steps:

- Choice of the substrate and its thickness to obtain the best performance in terms of loss.
- Design, and simulation of the BM components in microstrip lines. Phase shift is introduced by different lengths of transmission lines. Cross between the lines, change of layers and bends are also considered.
- Design, realization, and simulation of the microstrip-to-slotline transition as a key element in the proposed 4×6 BM.
- Design and simulation of the antenna element followed by the realization and simulation of the 6-element linear array.
- Design, fabrication and measurement of the complete network including the 4×6 BM integrated with the antenna array.

TABLE III
OVERALL PERFORMANCE OF THE 6-ELEMENT ARRAY FED BY THE BEAMFORMING NETWORK

	27.5 GHz				28 GHz				28.5 GHz			
	port1	port2	port3	port4	port1	port2	port3	port4	port1	port2	port3	port4
Beam Angle (deg)	$-14°$	$52°$	$-41°$	$13°$	$-13°$	$41°$	$-39°$	$13°$	$-13°$	$41°$	$-42°$	$13°$
HPBW (deg)	$17°$	$20°$	$21°$	$17°$	$17°$	$21°$	$18°$	$16°$	$16°$	$20°$	$23°$	$17°$
Realized Gain (dBi)	11.2	10.4	10.7	11.2	11.6	10.5	10.4	11.4	11.5	10.2	10.1	11.7
Cross-pol Level (dB)	-23	-23	-22	-22	-23	-21	-21	-22	-22	-22	-23	-22
Side-lobe Level (dB)	-17	-12	-11	-14.5	-16.5	-12.2	-12	-13.5	-15	-12.8	-11.6	-12

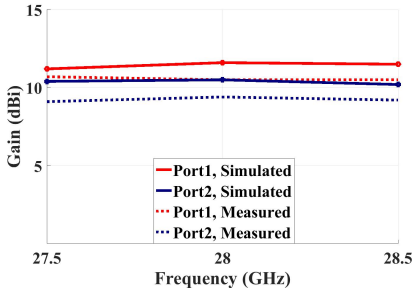

(a)

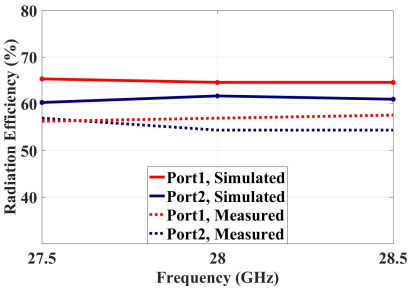

(b)

Fig. 19. Simulated and measured results when input ports 1 and 2 are excited. (a) Gain versus frequency. (b) Radiation efficiency versus frequency.

IV. EXPERIMENT AND MEASUREMENT RESULTS

Fig. 16 presents a prototype of the planar multi-beam antenna array which is fabricated with the use of the standard PCB process. Each layer is separately fabricated, then combined together using bonding film. The Rogers 5880 substrate with ϵ_r = 2.2, loss tangent = 0.0009 at 28 GHz and height = 0.127 mm is used for manufacturing both substrate layers.

A. Reflection and Isolation Coefficients

The scattering parameter measurements are performed using an Agilent Network Analyzer N5225A. The simulated and measured reflection and isolation coefficients are plotted in Fig. 17, and the results are in a good agreement. The graphs show that the return loss for port 1 to 4 excitations are better than -13 dB from 27.5 to 28.5 GHz, and the isolations are better than -15 dB within this band.

B. Radiation Pattern, Gain and Efficiency

The radiation patterns of the 28 GHz beamforming antenna array prototype are experimentally measured in an anechoic chamber with the use of far-field measurement system. Depending on the array's element spacing and number of elements, the intersection point between two adjacent beam has different levels, which displays the crossover level. Fig. 18 compares the simulated and measured pattern distribution for the entire network including the BM integrated with the antenna array at three different frequencies, 27.5, 28, and 28.5 GHz when different input ports are fed. The four beams are able to cover a wide azimuthal range roughly between $\pm 45°$. The radiation beams remain stable over the operating band from 27.5 to 28.5 GHz. It is noted that the crossover level is also displayed by these plots. Table III summarizes the overall performance of the simulated multi-beam antenna array. Fig. 19(a) and (b) compare the simulated and measured gain and radiation efficiency of the multi-beam antenna array versus frequency when input ports 1 and 2 are fed, respectively. The multi-beam antenna array structure is symmetric, so the beams of the input ports 3 and 4 are similar to those of the ports 1 and 2. The measured gains of the proposed network varies from 9.2 to 10.7 dBi at 28 GHz. The efficiency of the ports 1 and 2 calculated using simulated directivity and measured gain is better than 54.4%, 56.7% within the operating band, respectively. The difference between measured and simulated gain is less than 1.5 dB, and this deterioration is mainly attributed to bonding imperfection and fabrication tolerance. The mechanical process errors being taken into consideration, the measured and the simulated results agree well.

C. Comparison and Discussion

Geometry features and the key performance parameters of the reported BM and the overall beamforming antenna array have been compared with other designs and the results are presented in Table IV. Compared to 4×4 Butler matrices, this design has lower SLL. Three examples of non-conventional

TABLE IV
COMPARISON OF THE SIZE AND STRUCTURE OF THE PROPOSED BEAMFORMING ANTENNA ARRAY AND THOSE IN REFERENCES

Ref	Antenna array	Feed network configuration	Freq. range (GHz)	Radiation direction	SLL (dB)	Scan angle (deg)	X-pol level (dB)	RL (dB)	Gain (dB)	Overall network dimension (λ^2)	Size (BM) (λ^2)
[14]	Stepped Slot (1×4)	SIW (4×4)	33.3-41.7 (22.5%)	End-fire	-8	± 38	NG	> 12	10.4-12.8	$37.5\lambda \times 25\lambda$	$12.5\lambda \times 5\lambda$
[15]	Patch (2×4)	Microstrip (4×4)	57-64 (11.7%)	Broadside	NG	± 43	< -8	> 10	11-12	$6\lambda \times 5\lambda$	NG
[19]	Slot Array (6×4)	SIW (4×8)	15.7-16.3 (3.75%)	Broadside	-12	± 45	NG	> 23	20.6-22.7	$21\lambda \times 6.1\lambda$	$9\lambda \times 5.5\lambda$
[20]	Patch (8×10)	SIW (4×8)	37.5-38.5 (2.63%)	Broadside	-9	± 36	NG	> 10	19.8-22.1	$12.1\lambda \times 12\lambda$	$12.1\lambda \times 12\lambda$
[21]	Slot Array (1×8)	SIW (4×8)	27.5-28.5 (3.5%)	Broadside	-12	± 45	< -14	> 13	10.9-12.2	$8.2\lambda \times 4.1\lambda$	$6.1\lambda \times 4.1\lambda$
[22]	Slot Array (2×8)	SIW (8×8)	28-31 (10.2%)	Broadside	-10	± 55	NG	> 10	11-16	$13.5\lambda \times 6\lambda$	$10\lambda \times 4\lambda$
[23]	ME Dipole (1×8)	SIW (8×8)	50-77.8 (44%)	End-fire	-9	± 55	< -28	> 10	9-12	$22\lambda \times 16\lambda$	$15\lambda \times 8\lambda$
This work	Dipole (1×6)	Microstrip (4×6)	27.5-28.5 (3.5%)	End-fire	-10	± 45	< -22	> 13	9.2-11	$5.6\lambda \times 4.6\lambda$	$3.5\lambda \times 1.4\lambda$

⋆ **SLL:sidelobe level; RL:return loss; NG:not given**.

SIW Butler matrices analogous to this work are presented in [19]–[21], while their radiation pattern is broadside. This work proposes a simpler and smaller structure than the miniaturized 4×8 BM in [21], while the overall performance is not degraded. Compared to other designs using SIW, this design is based on microstrip, which is easier to be integrated with other components in systems, and there is no need for SIW to microstrip transition. This work is the smallest in reported multi-beam antenna arrays with Butler matrices with a compact size of $3.5\lambda \times 1.4\lambda$. The size of this work is much smaller than other reported multi-beam antenna arrays using Butler matrices with similar performance.

V. CONCLUSION

A mm-wave multi-beam antenna array using a novel realization of a 4×6 BM, connected to a 6-element planar linear antenna array has been described. The design provides a simple and compact structure potentially suitable for applications in mm-wave multi-beam communication systems. This has been ensured by a fully planar layout of a standard 4×4 BM appropriately connected with the use of two 3 dB power dividers and transmission-line crossovers to realize the 4×6 BM. The proposed concept has been verified by the measurement results of the fabricated prototype. The simulated and experimental outcomes agree well, and the obtained results confirm the attractive properties of the proposed network. This design is flexible to be extended to 4×8 BM, and as a result of which flexible crossover level is achievable. The results validate that the proposed array network can be a good candidate for 5G mm-wave applications.

REFERENCES

[1] T. S. Rappaport, S. Sun, R. Mayzus, H. Zhao, Y. Azar, K. Wang, G. N. Wong, J. K. Schulz, M. Samimi, and F. Gutierrez Jr, "Millimeter wave mobile communications for 5g cellular: It will work!" *IEEE Access*, vol. 1, no. 1, pp. 335–349, 2013.

[2] A. Gupta and R. K. Jha, "A survey of 5g network: Architecture and emerging technologies," *IEEE access*, vol. 3, pp. 1206–1232, 2015.

[3] M. Than, "Billion connected devices," *White Paper, (ERICSSON, 2013)*, 50.

[4] J. G. Andrews, S. Buzzi, W. Choi, S. V. Hanly, A. Lozano, A. C. Soong, and J. C. Zhang, "What will 5g be?" *IEEE Journal on selected areas in communications*, vol. 32, no. 6, pp. 1065–1082, 2014.

[5] C. N. Barati, S. A. Hosseini, M. Mezzavilla, T. Korakis, S. S. Panwar, S. Rangan, and M. Zorzi, "Initial access in millimeter wave cellular systems," *IEEE Trans. Wireless Commun.*, vol. 15, no. 12, pp. 7926–7940, 2016.

[6] W. El-Halwagy, R. Mirzavand, J. Melzer, M. Hossain, and P. Mousavi, "Investigation of wideband substrate-integrated vertically-polarized electric dipole antenna and arrays for mm-wave 5g mobile devices," *IEEE Access*, vol. 6, pp. 2145–2157, 2018.

[7] W. Hong, Z. H. Jiang, C. Yu, J. Zhou, P. Chen, Z. Yu, H. Zhang, B. Yang, X. Pang, M. Jiang *et al.*, "Multibeam antenna technologies for 5g wireless communications," *IEEE Trans. Antennas Propag.*, vol. 65, no. 12, pp. 6231–6249, 2017.

[8] W. Hong, K.-H. Baek, and S. Ko, "Millimeter-wave 5g antennas for smartphones: Overview and experimental demonstration," *IEEE Trans. Antennas Propag.*, vol. 65, no. 12, pp. 6250–6261, 2017.

[9] J. Helander, K. Zhao, Z. Ying, and D. Sjöberg, "Performance analysis of millimeter-wave phased array antennas in cellular handsets," *IEEE Antennas Wireless Propag. Lett.*, vol. 15, pp. 504–507, 2016.

[10] J. Nolen, "Synthesis of multiple beam networks for arbitrary illuminations," *Bendix*, 1965.

[11] S. Mosca, F. Bilotti, A. Toscano, and L. Vegni, "A novel design method for blass matrix beam-forming networks," *IEEE Trans. Antennas Propag.*, vol. 50, no. 2, pp. 225–232, 2002.

[12] W. Rotman and R. Turner, "Wide-angle microwave lens for line source applications," *IEEE Trans. Antennas Propag.*, vol. 11, no. 6, pp. 623–632, 1963.

[13] J. Butler, "Beam-forming matrix simplifies design of electronically scanned antenna," *Electron. Design*, vol. 9, pp. 170–173, 1961.

[14] Q. Wu, J. Hirokawa, J. Yin, C. Yu, H. Wang, and W. Hong, "Millimeter-wave multi-beam end-fire dual circularly polarized antenna array for 5g wireless applications," *IEEE Trans. Antennas Propag.*, vol. 66, no. 9, pp. 4930–4935, 2018.

[15] W. F. Moulder, W. Khalil, and J. L. Volakis, "60-ghz two-dimensionally scanning array employing wideband planar switched beam network," *IEEE Antennas Wireless Propag. Lett.*, vol. 9, pp. 818–821, 2010.

[16] M. Nedil, T. A. Denidni, and L. Talbi, "Novel butler matrix using cpw multilayer technology," *IEEE Trans. Microw. Theory Techn.*, vol. 54, no. 1, pp. 499–507, 2006.

[17] C. Dall'Omo, T. Monediere, B. Jecko, F. Lamour, I. Wolk, and M. Elkael, "Design and realization of a 4× 4 microstrip butler matrix without any crossing in millimeter waves," *Microwave and Optical Technology Letters*, vol. 38, no. 6, pp. 462–465, 2003.

[18] S. Gruszczynski, K. Wincza, and K. Sachse, "Reduced sidelobe four-beam n-element antenna arrays fed by $4 \times n$ butler matrices," *IEEE Antennas Wireless Propag. Lett.*, vol. 5, no. 1, pp. 430–434, 2006.

[19] P. Chen, W. Hong, Z. Kuai, J. Xu, H. Wang, J. Chen, H. Tang, J. Zhou, and K. Wu, "A multibeam antenna based on substrate integrated waveguide technology for mimo wireless communications," *IEEE Trans. Antennas Propag.*, vol. 57, no. 6, pp. 1813–1821, 2009.

[20] Y. Cao, K.-S. Chin, W. Che, W. Yang, and E. S. Li, "A compact 38 ghz multibeam antenna array with multifolded butler matrix for 5g applications," *IEEE Antennas Wireless Propag. Lett.*, vol. 16, pp. 2996–2999, 2017.

[21] J.-W. Lian, Y.-L. Ban, C. Xiao, and Z.-F. Yu, "Compact substrate-integrated 4× 8 butler matrix with sidelobe suppression for millimeter-wave multibeam application," *IEEE Antennas Wireless Propag. Lett.*, vol. 17, no. 5, pp. 928–932, 2018.

[22] L.-H. Zhong, Y.-L. Ban, J.-W. Lian, Q.-L. Yang, J. Guo, and Z.-F. Yu, "Miniaturized siw multibeam antenna array fed by dual-layer 8× 8 butler matrix," *IEEE Antennas Wireless Propag. Lett*, vol. 16, pp. 3018–3021, 2017.

[23] Y. Li and K.-M. Luk, "A multibeam end-fire magnetoelectric dipole antenna array for millimeter-wave applications," *IEEE Trans. Antennas Propag.*, vol. 64, no. 7, pp. 2894–2904, 2016.

[24] K. Wincza, S. Gruszczynski, and K. Sachse, "Broadband planar fully integrated 8×8 butler matrix using coupled-line directional couplers," *IEEE Trans. Microw. Theory Techn.*, vol. 59, no. 10, pp. 2441–2446, 2011.

[25] A. Abbosh, "Wideband planar crossover using two-port and four-port microstrip to slotline transitions," *IEEE Microw. Wireless Compon. Lett.*, vol. 22, no. 9, pp. 465–467, 2012.

[26] B. Shuppert, "Microstrip-slotline transitions: Modeling and experimental investigation," *IEEE Trans. Microw. Theory Techn.*, vol. 36, no. 8, pp. 1272–1282, 1988.

[27] N. Seman and M. E. Bialkowski, "Microstrip-slot transition and its applications in multilayer microwave circuits," in *Passive microwave components and antennas*. InTech, 2010.

[28] B.-K. Tan, S. Withington, and G. Yassin, "A compact microstrip-fed planar dual-dipole antenna for broadband applications," *IEEE Antennas Wireless Propag. Lett.*, vol. 15, pp. 593–596, 2016.

[29] N. Kaneda, W. Deal, Y. Qian, R. Waterhouse, and T. Itoh, "A broadband planar quasi-yagi antenna," *IEEE Trans. Antennas Propag.*, vol. 50, no. 8, pp. 1158–1160, 2002.

[30] R. J. Mailloux, *Phased array antenna handbook*. Artech House Boston, 2005, vol. 2.

Maral Ansari (S'17) was born in Mashhad, Iran, in 1990. She received the M.S. degree in electrical and communication engineering from Tabriz University, Tabriz, Iran, in 2015. She is currently pursuing the Ph.D. degree in electrical engineering with the Global Big Data Technologies Centre, School of Electrical and Data Engineering in the Faculty of Engineering and IT at the University of Technology Sydney (UTS), Sydney, NSW, Australia. Her current research interests include mm-wave antenna arrays, multi-beam scanning and beamforming networks.

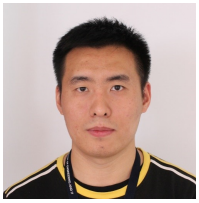

He Zhu received the B.Sc degree and M.Eng degree from South China University of Technology, Guangzhou, China, and Ph.D. degree in Electrical Engineering from the School of ITEE, University of Queensland, Brisbane, Australia. He is currently a Post-doctoral Research Fellow with Global Big Data Technologies Centre (GBDTC), University of Technology Sydney (UTS), Australia. His research interests include development of passive and tunable microwave and mm-wave devices, radio frequency integrated circuits and systems, and beam-forming networks for antenna arrays.

Negin Shariati completed her PhD in Electrical-Electronic and Communication Technologies at Royal Melbourne Institute of Technology (RMIT), Australia in 2016. She worked in industry as an Electrical-Electronic Engineer from 2009-2012. Dr Negin Shariati joined the School of Electrical and Data Engineering in the Faculty of Engineering and IT at the University of Technology Sydney (UTS), Australia in 2016 as a Lecturer. She is also a Lecturer at Hokkaido University since 2018, externally engaging with research and teaching activities in Japan. Dr Negin Shariati established the state of the art RF and Communication Technologies (RFCT) research lab at UTS in 2018, where she is currently the Deputy Director and leads the research direction and strategy of the lab. Her research interests are in RF energy harvesting, Self-powered electronic systems for IoT devices, Simultaneous wireless information and power transfer, Nonlinear device modeling, and Renewable energy systems. She is the recipient of the IEEE Victorian Section Best Research Paper Award 2015, RMIT Higher Degree by Research (HDR) Publication Grant 2015, the Boeing Scholarship 2013, Research Paper Grants at European Microwave Conferences 2012, 2014 and 2015, the Best Oral Presentation Prize at RMIT HDR Conference 2012, and RMIT Postgraduate Research Scholarship.

Y. Jay Guo (Fellow'2014) received a Bachelor Degree and a Master Degree from Xidian University in 1982 and 1984, respectively, and a PhD Degree from Xian Jiaotong University in 1987, all in China. His research interest includes antennas, mm-wave and THz communications and sensing systems as well as big data technologies. He has published over 450 research papers and holds 26 patents in antennas and wireless systems. He is a Fellow of the Australian Academy of Engineering and Technology, a Fellow of IEEE and a Fellow of IET, and was a member of the College of Experts of Australian Research Council (ARC, 2016-2018). He has won a number of most prestigious Australian national awards, and was named one of the most influential engineers in Australia in 2014 and 2015, respectively.

Prof Guo is a Distinguished Professor and the founding Director of Global Big Data Technologies Centre (GBDTC) at the University of Technology Sydney (UTS), Australia. Prior to this appointment in 2014, he served as a Director in CSIRO for over nine years, directing a number of ICT research portfolios. Before joining CSIRO, he held various senior technology leadership positions in Fujitsu, Siemens and NEC in the U.K.

Prof Guo has chaired numerous international conferences. He is the Chair Elect of International Steering Committee, International Symposium on Antennas and Propagation (ISAP). He was the International Advisory Committee Chair of IEEE VTC2017, General Chair of ISAP2015, iWAT2014 and WPMC'2014, and TPC Chair of 2010 IEEE WCNC, and 2012 and 2007 IEEE ISCIT. He served as Guest Editor of special issues on "Antennas for Satellite Communications" and "Antennas and Propagation Aspects of 60-90GHz Wireless Communications," both in IEEE Transactions on Antennas and Propagation, Special Issue on "Communications Challenges and Dynamics for Unmanned Autonomous Vehicles," IEEE Journal on Selected Areas in Communications (JSAC), and Special Issue on "5G for Mission Critical Machine Communications", IEEE Network Magazine.